10.3   **COMPARISON OF POLARIMETRIC ALGORITHMS FOR HYDROMETEOR CLASSIFICATION AT S AND C BANDS**

A.   Ryzhkov[1], D. Zrnic[2], P. Zhang[1], J. Krause[1], H. Park[3], D. Hudak[4], J. Young[4], J. L. Alford[5], M. Knight[5], J. W. Conway[6].

(1) CIMMS / OU, (2) NSSL, (3) Kyungpook National University, (4) Environment Canada, (5) Enterprise Electronics Corporation, (6) Weather Decisions Technology.

1. INTRODUCTION

Dual-polarization radar is a unique instrument for classification of radar echo. Different versions of the classification algorithm based on the principles of fuzzy logic are described in a number of papers (Zrnic and Ryzhkov 1999, Vivekanandan et al. 1999, Liu and Chandrasekar 2000, Zrnic et al. 2001, Keenan 2003, Lim et al. 2005). Initially the classification techniques have been developed and tested at S band. Adaptation of classification routine for C band requires some special considerations mainly because of the more pronounced effects of resonance scattering and stronger attenuation at this shorter wavelength.

In this paper, we briefly describe the S-band classification algorithm which is going to be implemented on polarimetric WSR-88Ds and examine the differences between classification routines at S and C bands using S-band data collected in Oklahoma and C-band data obtained in Alabama and Southern Ontario, Canada.

2. NEXRAD CLASSIFICATION ALGORITHM

The suggested classification algorithm distinguishes between 10 classes of radar echo: (1) ground clutter / anomalous propagation (GC/AP), (2) biological scatterers (BS), (3) dry aggregated snow (DS), (4) wet snow (WS), (5) crystals of different orientation (CR), (6) graupel (GR), (7) "big drops" (BD), (8) light and moderate rain (RA), (9) heavy rain (HR), and (10) rain / hail mixture (RH). The algorithm utilizes six radar variables: radar reflectivity at horizontal polarization Z, differential reflectivity Z_{DR}, cross-correlation coefficient ρ_{hv}, specific differential phase K_{DP}, and the texture parameters of radar reflectivity SD(Z) and differential phase SD(Φ_{DP}). These six variables are directly used in a fuzzy logic classification scheme. Additional Doppler variable, mean Doppler velocity V, is utilized for discrimination between hail and ground clutter / AP, although it is not included in the set of input variables for the fuzzy logic classifier.

The aggregation values or scores for each of 10 classes are determined as

Corresponding author address: Alexander Ryzhkov, CIMMS/NSSL, Norman, Oklahoma, USA; Email: Alexander.Ryzhkov@noaa.gov

$$A_i = \frac{\sum_{j=1}^{6} W_{ij} Q_j P^{(i)}(V_j)}{\sum_{j=1}^{6} W_{ij} Q_j} \quad , \quad (1)$$

where $P^{(i)}(V_j)$ is a membership function of the jth variable for i^{th} class, W_{ij} is a weight between 0 and 1 assigned to the ith class and j^{th} variable, and Q_j is an element of the confidence vector characterizing instrumental quality of the measurement of the jth variable. The type of radar echo is identified by the maximal aggregation value.

Matrix of weights **W** characterizes classification efficiency of each variable with respect to a particular class. The procedure for determining the elements of matrix **W** is described in Park et al. (2007).

For each range location, every radar variable is supplemented with its confidence factor Q_j depending on its vulnerability to (a) attenuation, (b) effects of nonuniform beam filling, (c) magnitude of ρ_{hv} (which determines statistical measurement errors of all polarimetric variables), (d) signal-to-noise ratio SNR, and severity of the four mentioned factors.

As an example, the Z_{DR} component of the confidence vector can be expressed as

$$Q_{Zdr} = \exp\left\{-0.69\left[\left(\frac{\Phi_{DP}}{\Phi_{DP}^{(Zdr)}}\right)^2 + \left(\frac{\Delta Z_{DR}}{\Delta Z_{DR}^{(t)}}\right)^2 + \left(\frac{1-\rho_{hv}}{\Delta\rho_{hv}^{(1)}}\right)^2 + \left(\frac{snr^{(Zdr)}}{snr}\right)^2\right]\right\}$$

$$(2)$$

In (2), Φ_{DP} is measured differential phase, ρ_{hv} is measured cross-correlation coefficient, $snr = 10^{0.1SNR}$ is signal-to-noise ratio in linear scale, ΔZ_{DR} is the Z_{DR} bias caused by nonuniform beam filling (NBF), and $\Phi_{DP}^{(Zdr)}$, $\Delta Z_{DR}^{(t)}$, $\Delta\rho_{hv}^{(1)}$, $snr^{(Zdr)}$ are threshold parameters. The NBF-related Z_{DR} bias is computed from gradient estimates as specified by Ryzhkov (2007). If the impact of attenuation and NBF is negligible (Φ_{DP} and ΔZ_{DR} are low), $\rho_{hv} \approx 1$, and SNR is high, then the value of Q_{Zdr} is close to 1, i.e., Z_{DR} can be used with full confidence. The confidence in the Z_{DR} measurement decreases as Φ_{DP} and ΔZ_{DR} increase and ρ_{hv} and SNR decrease.

Because membership functions of some classes of liquid and frozen hydrometeors (such as rain and dry snow) heavily overlap, class designation should be contingent on the localization of the melting layer. The melting layer detection algorithm developed at NSSL determines the top and bottom of the melting layer as functions of azimuth for any given radar scan (Giangrande et al. 2007). The parameters of the melting layer are estimated from the measurements at higher elevations between 4 and 10º.

Checking the consistency of the designated class with the location of the melting layer is important integral part of classification routine. The geometry of the radar beam with respect to the melting layer is illustrated in Fig. 1. Slant ranges R_b and R_t correspond to geometrical projections of the melting layer from the beam axis to the ground, and $R_t - R_b$ indicates the range extent of the melting layer along an infinitesimally thin beam. In fact, mixed-phase hydrometeors may partially fill the radar resolution volume in a much broader interval of ranges (R_{bb},R_{tt}) if the antenna beam has finite width.
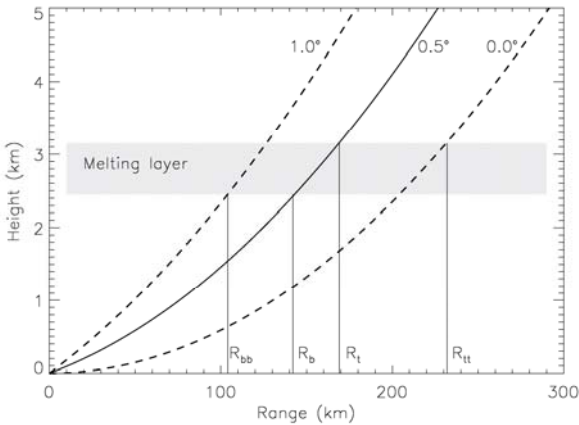

Fig. 1. The geometry of radar beam with respect to the melting layer.

Certain subsets of classes are allowed within five slant range intervals shown in Fig. 1:

$0 < R < R_{bb}$ GC/AP, BS, BD, RA, HR, RH

$R_{bb} < R < R_b$ GC/AP, BS, WS, GR, BD, RA, HR, RH

$R_b < R < R_t$ GC/AP, BS, DS, WS, GR, BD, RH

$R_t < R < R_{tt}$ GC/AP, BS, DS, WS, CR, GR, BD, RH

$R > R_{tt}$ DS, CR, GR, RH

For example, the highest aggregation score among the following 6 classes (GC/AP, BS, BD, RA, HR, RH) determines the class designation if $R < R_{bb}$ (even if DS scores highest score among all 10 classes at the distance R).

Additional routines in the classification algorithm include separation of convective and stratiform echo, "sanity" checks, and despeckling. Identifying convective and stratiform parts of radar echo helps to better discriminate between wet snow and melting graupel within the melting layer. The set of "sanity "checks or "hard-threshold" conditions is used to reduce the number of apparently wrong class designations, e.g., hail is definitely wrongly classified if Z < 30 dBZ, etc. Despeckling procedure reduces the noisiness in the fields of classification results.

An example of the composite plot of Z, Z_{DR}, ρ_{hv}, and results of classification for the most recent version of the

proposed NEXRAD classification algorithm is shown in Fig. 2.

3. RADAR ECHO CLASSIFICATION AT C BAND

3.1 *Resonance scattering at C band*

If atmospheric hydrometeors were much smaller compared to the radar wavelength and behaved as Rayleigh scatterers both at S and C band, then the only difference between radar variables at the two wavelengths would be in K_{DP} which is inversely proportional to the wavelength. However, at C band, raindrops with sizes exceeding 4.5 – 5 mm are large enough to cause pronounced effects of resonance scattering, i.e., they behave as Mie scatterers. Hence, if sufficiently large drops exist in the raindrop spectrum, then both radar reflectivity factor Z and differential reflectivity Z_{DR} can be noticeably higher at C band than at S band.

Our simulations based on DSD measurements in Oklahoma indicate that for the same rain the difference in Z between S and C band can be as high as 5 dB and the Z_{DR} difference can exceed 3 dB. Theoretical values of the cross-correlation coefficient ρ_{hv} for the measured DSDs are always above 0.98 at S band and can drop as low as 0.93 at C band (Ryzhkov and Zrnic 2005). Such low values of ρ_{hv} at S band would most likely result in the nonrain class designation.

3.2 *Hail detection at C band*

At S band, hail is identified if high Z is accompanied by low Z_{DR} or, in a more quantitative way, if the Hail Differential Reflectivity parameter HDR = Z – f(Z_{DR}) exceeds certain threshold (Aydin et al. 1986).

If large raindrops with very high Z_{DR} at C band are mixed with hail whose intrinsic Z_{DR} is close to zero, the resulting Z_{DR} may remain quite high even if significant amount of hail is present in the mixture. Our detailed analysis of strong reflectivity cores in 11 summer storms observed in Southern Ontario and Alabama with C-band radars has not revealed any noticeable drop in Z_{DR} in the areas of very high Z where hail was reported on the ground. It is likely that the HDR technique for discrimination between rain and hail proven efficient at S band might not be applicable at C band.

Hail-bearing regions in the storms may produce anomalously high differential attenuation which results in a tremendous drop of Z_{DR} on the rear side of hail cell, but if such differential attenuation is correctly accounted for, the unbiased Z_{DR} remains high everywhere in the cell (Ryzhkov et al. 2007). It is possible that insufficient correction of Z_{DR} for differential attenuation might have caused artificially large HDR (which is in fact quite low) in the past studies of polarimetric hail detection at C band.

We speculate that the joint use of Z and K_{DP} might be more efficient for hail detection at C band than the combination of Z and Z_{DR}. This point is illustrated in Fig. 2 and 3 where the scatterplots of ρ_{hv}, Z_{DR}, and $10\log(K_{DP})$ versus Z are displayed for the cases of extended band of heavy rain with little hail and localized storm which produced golf ball size hail. Both
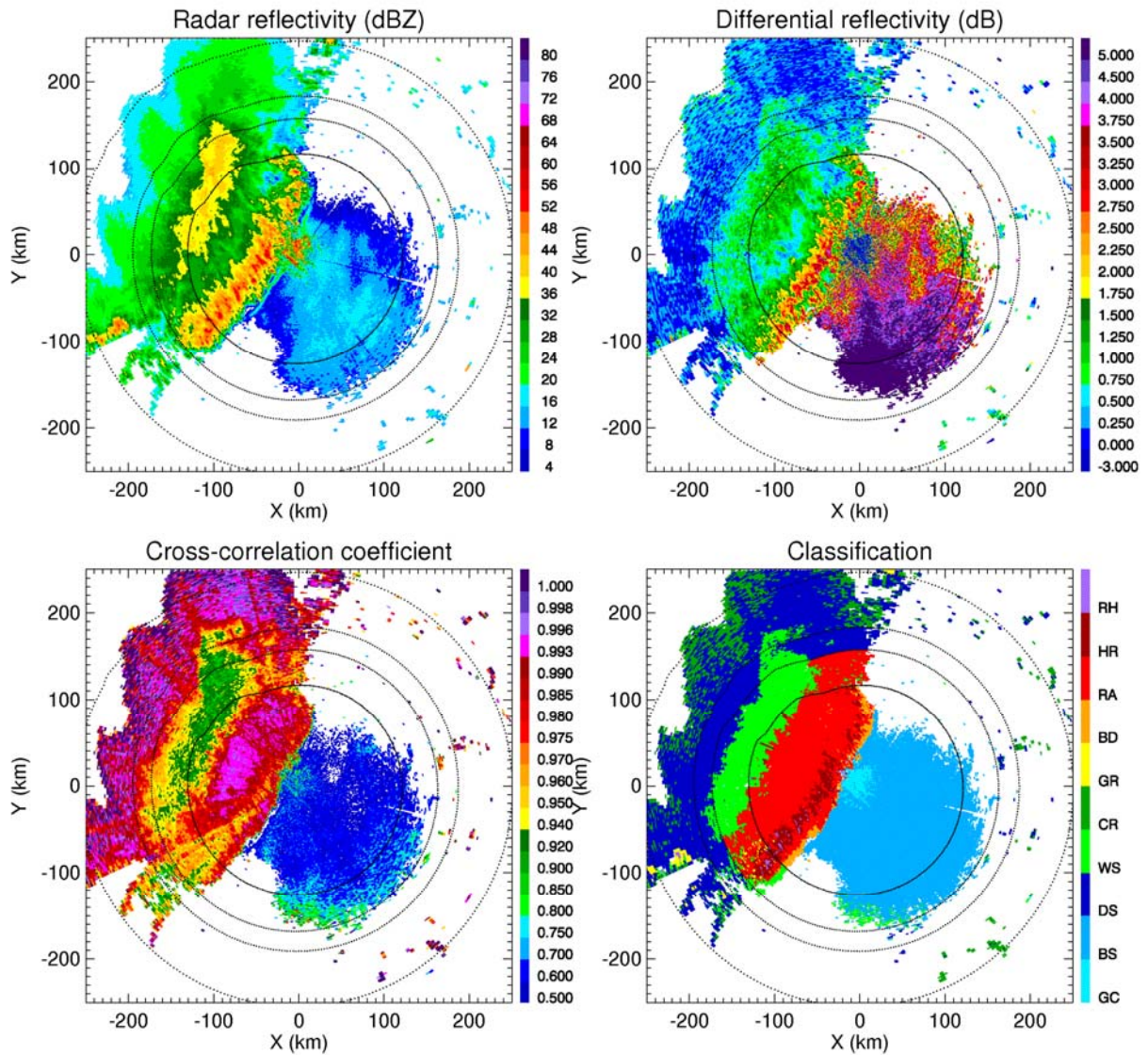
Fig. 2. Composite plot of Z, Z_{DR}, ρ_{hv}, and results of classification obtained from the polarimetric prototype of the WSR-88D radar on 05/13/2005, 0659 UTC, El = 0.5°. Contours in the plots indicate slant ranges R_{bb}, R_b, R_t, R_{tt} as functions of azimuth. In the classification panel, GC stands for ground clutter, BS – for biological scatterers, DS – for dry snow, WS – for wet snow, CR – for crystals, GR – for graupel, BD – for "big drops", RA – for rain (light and moderate), HR – for heavy rain, and RH – for rain / hail mixture.

observations have been made in Ontario with the C-band King radar.

These scatterplots are very typical. Extended storms (e.g., squall lines, MCSs) producing plenty of rain usually contain large number of small drops, therefore their Z_{DR} is quite low and ρ_{hv} is generally high (Fig. 3). Occasional small hail in such storms may exhibit slight decrease in Z_{DR}, ρ_{hv}, and K_{DP} at high reflectivities (exceeding 50 dBZ). The corresponding values of Z_{DR} and K_{DP} apparently deviate from the major "rain" cluster confined between the boundaries in Fig. 3 and 4 defined by equations

$$Z_{DR} = -0.04 - 0.012\,Z + 0.00064\,Z^2 \qquad (3)$$

$$Z_{DR} = 0.56 - 0.0066\,Z + 0.0011\,Z^2 \qquad (4)$$

$$10\log(K_{DP}) = -42.9 + 0.926\,Z \qquad (5)$$

$$10\log(K_{DP}) = -37.9 + 0.926\,Z \qquad . \qquad (6)$$

In the case of a localized storm which produced large hail, the drop in ρ_{hv} and K_{DP} at Z > 45 dBZ is more dramatic (Fig. 4). On the contrary, Z_{DR} substantially increases at high Z. Similar increase in Z_{DR} in the periphery of strong hail cores is often observed at S band and is usually attributed to melting hail. The important difference between polarimetric hail signatures at C and S bands is that even in the middle of hail shaft large tumbling hail with intrinsic near-zero Z_{DR} generally does not offset the contribution from
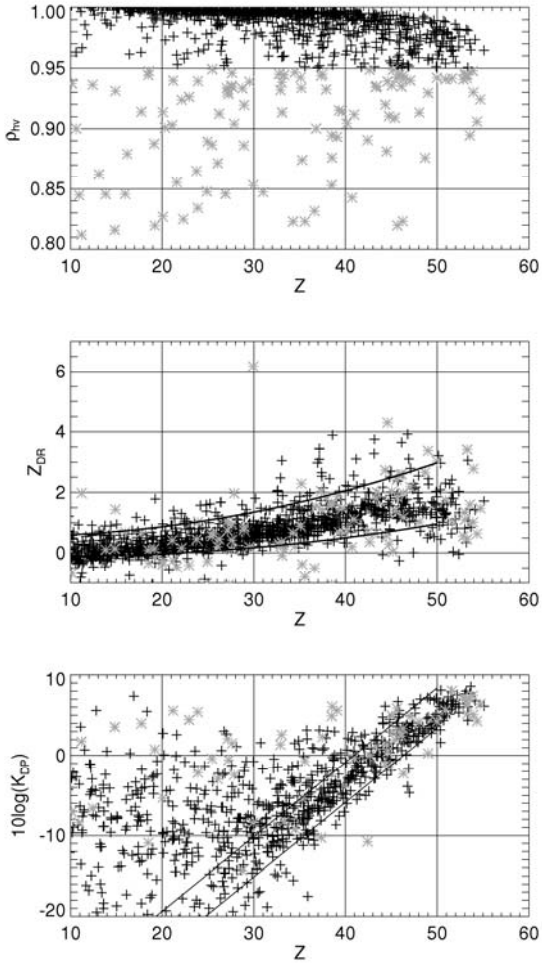
Fig. 3. The scatterplots of ρ_{hv}, Z_{DR}, and 10 log (K_{DP}) versus Z at C band from the data collected with the King radar in Southern Ontario on 08/19/2005, 1730 UTC. Grey asterisks correspond to ρ_{hv} < 0.95. The storm caused flash flood in the Toronto area.

Fig. 4. Same as in Fig. 3 but for the hailstorm observed in Ontario on 06/14/2005, 2220 UTC. The storm produced golf ball size hail.

smaller melting hail and large raindrops which produce anomalously high Z_{DR} at C band.

Ryzhkov et al. (2007) report anomalously high differential attenuation at C band which is commonly observed in the "hotspots" associated with hail. The C-band algorithm for attenuation correction suggested by Ryzhkov et al (2007) estimates the ratio β of specific differential attenuation A_{DP} and K_{DP} in such "hotspots". Since this ratio tends to increase in the presence of hail of larger size, the parameter β can be added to the set of polarimetric variables which are traditionally used for hydrometeor classification.

3.3 *Quality of polarimetric measurements at C band*

Such radar variables as Z, Z_{DR}, and ρ_{hv} are more affected by attenuation and nonuniform beam filling at shorter radar wavelengths (Ryzhkov 2007). In addition, ρ_{hv} is generally lower at C band due to resonance scattering which results in increasing noisiness of all polarimetric variables. These factors should be taken into account in defining the confidence vector Q characterizing the quality of radar measurements in Eq(1).
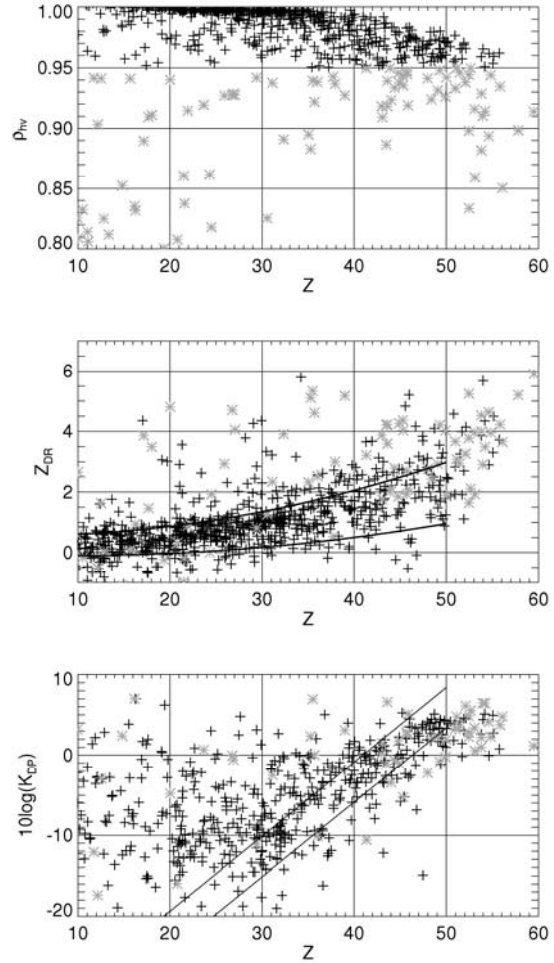
Generally speaking, K_{DP} should be given larger classification role at shorter radar wavelength, because it is immune to attenuation. On the other hand, Z_{DR} should be utilized more cautiously at C band because it is so much affected by effects of resonance scattering and differential attenuation.

We also noticed stronger impact of NBF on the magnitude of ρ_{hv} at C band. Such an impact manifests itself as a significant drop in ρ_{hv} if the gradient of total differential phase is too high. Negatively biased ρ_{hv} detrimentally affects the quality of classification, therefore, the confidence factor for ρ_{hv} has to be lowered in the regions of pronounced NBF.

3.4 *Examples of classification at C band*

The S-band classification code has been adapted for C band following considerations described above. Numerous changes in the membership functions, matrix of weights, and confidence vector have been made. The classification algorithm has been extensively tested on
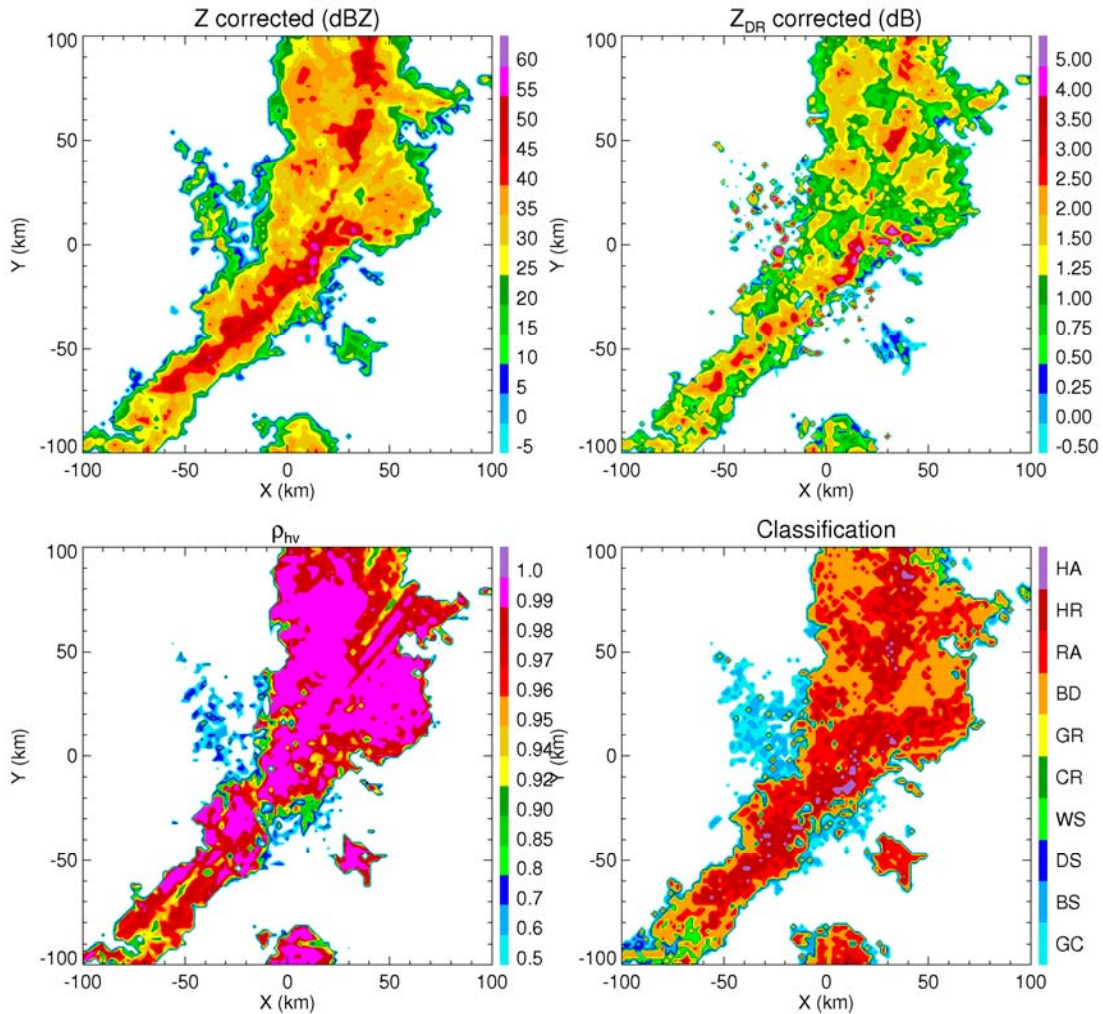
Fig. 5. Composite plot of Z, Z_{DR}, ρ_{hv}, and results of classification obtained from the C-band King radar on 04/23/2007, 2020 UTC, El = 0.5º. Class notations are the same as in Fig. 2.

the C-band data collected in Canada and Alabama. Two examples are provided to illustrate the algorithm skills.

One example is an extended line of heavy rain sporadically mixed with hail observed in Ontario on 04/23/2007. This storm produced tremendous attenuation (up to 40 dB) and differential attenuation (up to 13 dB) quantified in Ryzhkov et al. (2007). Hence, successful classification heavily relies on the adequate attenuation correction. The classification algorithm detects small areas of hail which was confirmed on the ground SE of the radar. The area of ground clutter associated with the ridge NW of the radar location is also correctly identified.

Second example is presented for the devastating tornadic storm in Alabama on 03/01/2007. This storm caused horrendous destruction and loss of life in the city of Enterprise where the Sidpol C-band radar is located (Conway et al. 2007). Large-scale plots of radar reflectivity and results of classification are shown in Fig. 6, whereas the corresponding images with higher resolution and smaller scale are presented in Fig. 7. Again, the classification code efficiently recognizes hail in the area of forward-flank downdraft in the supercell

part of the storm and the echo from biological scatterers and ground clutter surrounding the radar. It is quite difficult to delineate the echoes from nonmeteorological and meteorological scatterers in the close proximity to the radar based on radar reflectivity only (Fig. 7). The classification routine clearly separates them. It is interesting that the algorithm identifies a tornadic debris echo associated with isolated spot of high reflectivity 4 km west of the radar as nonmeteorological, namely, ground clutter.

At the moment, we are hesitant to include a special class "tornadic debris" in the current version of our classification scheme because polarimetric characteristics of tornadic debris and ground clutter are very similar. The distinction between the two can be based on localization of the signature (hook echo), and on the analysis of Doppler variables such as mean Doppler velocity and Doppler vortex signature. In addition, other polarimetric signatures characterizing tornadic supercell storms should be taken into account (Kumjian and Ryzhkov 2007).
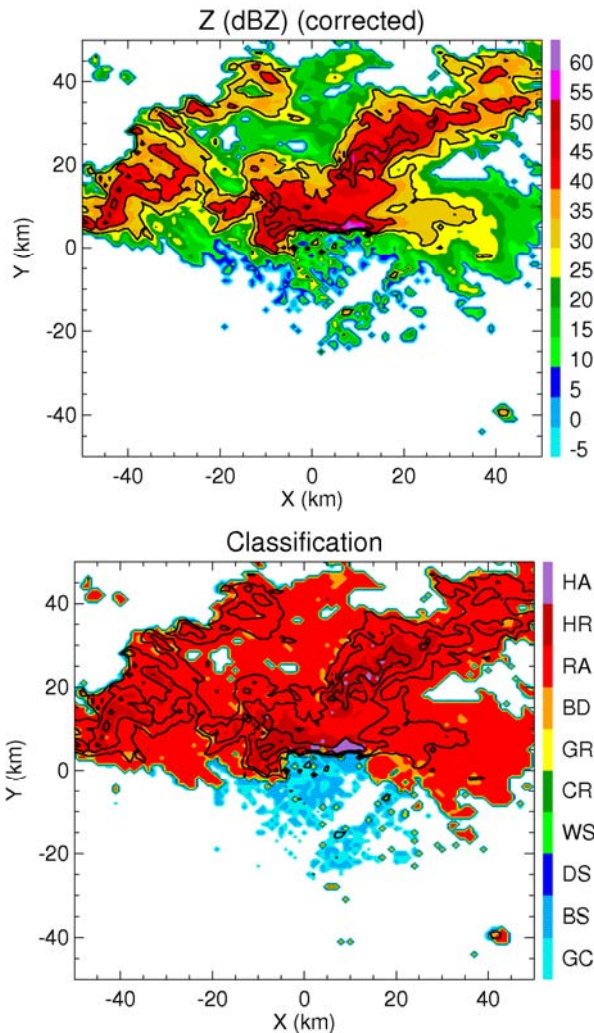
Fig. 6. Composite plot of radar reflectivity and results of classification for the Enterprise tornadic storm on 03/01/2007, 1908 UTC, El = 0.5º. Overlaid are contours of Z = 30 dBZ.
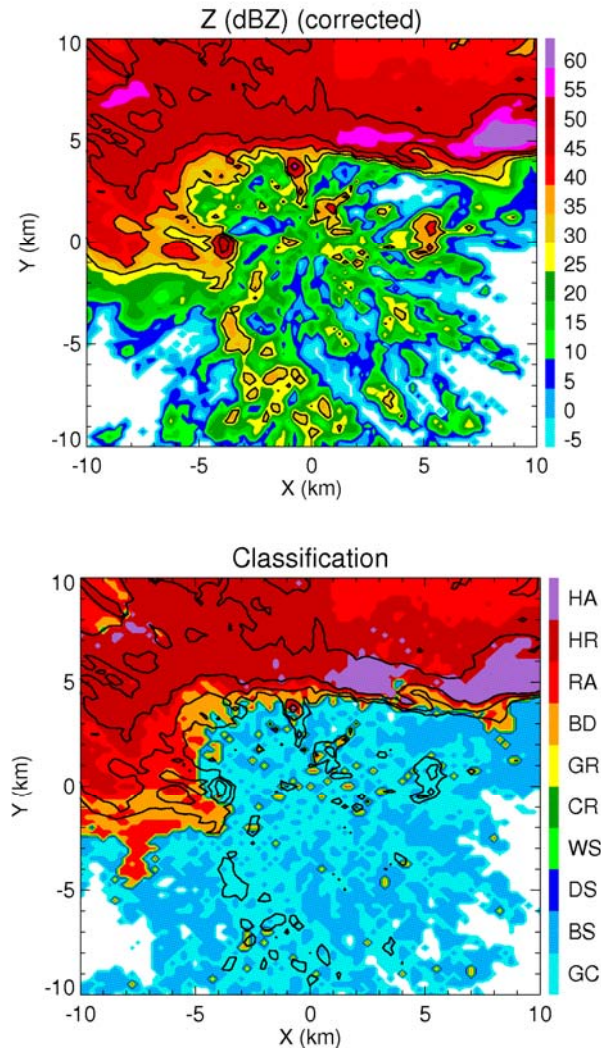
Fig. 7. Same as in Fig. 6 but at smaller scale. Tornado is located at X = - 4 km, Y = 0 km. The Sidpol radar is in the center of image.

REFERENCES

Aydin, K., T. Seliga, and V. Balaji, 1986: Remote sensing of hail with a dual linear polarization radar. *J. Climate Appl. Meteor.*, **25**, 1475 – 1484

Conway, J.W., A. V. Ryzhkov, E.D. Mitchell, P. Zhang, L. Venkatramani, J. L. Alford, and D. Nelson, 2007: Examination of tornadic signatures observed at very close range using simultaneous dual-polarization radar at C band. Preprints, *33rd Conf. on Radar Meteorology,* CD-ROM, P10.2.

Giangrande, S., J. Krause, and A. Ryzhkov, 2007: Automatic designation of the melting layer with a polarimetric prototype of the WSR-88D radar. Submitted to *J.Appl. Meteor..*

Keenan, T.D., 2003: Hydrometeor classification with a C-band polarimetric radar. *Aust. Meteor. Mag.*, **52**, 23 – 31.

Kumjian, M. and A. Ryzhkov, 2007: Polarimetric characteristics of tornadic and nontornadic suprecell storms. Preprints, *33rd Conf. on Radar Meteorology,* CD-ROM, P10.1.

Lim, S., V. Chandrasekar, and V.N. Bringi, 2005: Hydrometeor classification system using dual-polarization radar measurements: model improvements and in situ verification. *IEEE Trans. Geosci. Rem. Sens.*, **43**, 792 – 801.

Liu, H., and V. Chandrasekar, 2000: Classification of hydrometeors based on polarimetric radar measurements: Development of fuzzy logic and neuro-fuzzy systems, and in situ verification. *J. Atmos. Oceanic Technol.,* **17**, 140–164.

Park, H.-S., A. Ryzhkov, D. Zrnic, and K. Kim, 2007: Optimization of the matrix of weights in the polarimetric algorithm for classification of radar echoes. Preprints, *33rd Conf. on Radar Meteorology,* CD-ROM, P11B.4.

Ryzhkov, A., 2007: The impact of beam broadening on the quality of radar polarimetric data. *J. Atmos. Oceanic Technol*, **24**, 729 – 744.

Ryzhkov, A., and D. Zrnic, 2005: Radar polarimetry at S, C, and X bands. Comparative analysis and operational implications. Preprints, *32nd Conference on Radar Meteorology.*, CD-ROM, 9R.3.

Ryzhkov, A., P. Zhang, D. Hudak, J.L. Alford, M. Knight, and J.W. Conway, 2007: Validation of polarimetric methods for attenuation correction at C band. Preprints, *33rd Conerence. on Radar Meteorology.*, CD-ROM, P11B.12.

Vivekanandan, J., D. Zrnic*,* S. Ellis, D. Oye, A. Ryzhkov, J. Straka, 1999: Cloud microphysics retrieval using S-band dual-polarization radar measurements. *Bull. Amer. Meteor. Soc.,* **80**, 381-388.

Zrnic, D., and A. Ryzhkov, 1999 Polarimetry for weather surveillance radars. *Bull. Amer. Meteor. Soc.,* **80**, 389 - 406.

Zrnic, D.S., A.V. Ryzhkov, J. Straka, Y. Liu, and J. Vivekanandan, 2001: Testing a procedure for the automatic classification of hydrometeor types. *J. Atmos. Oceanic Technol.*, **18**, 892 – 913.